Applied Physics Letters

Tamm plasmon sub-wavelength structuration for loss reduction and resonance tuning

Cite as: Appl. Phys. Lett. **111**, 261103 (2017); https://doi.org/10.1063/1.4991025
Submitted: 19 June 2017 • Accepted: 10 December 2017 • Published Online: 27 December 2017

A. R. Gubaydullin, C. Symonds, J.-M. Benoit, et al.

Tamm plasmon sub-wavelength structuration for loss reduction and resonance tuning

A. R. Gubaydullin,[1,2,a)] C. Symonds,[1,a)] J.-M. Benoit,[1] L. Ferrier,[3] T. Benyattou,[3] C. Jamois,[3] A. Lemaître,[4] P. Senellart,[4] M. A. Kaliteevski,[5] and J. Bellessa[1,a)]
[1]*Univ Lyon, Université Claude Bernard Lyon 1, CNRS, Institut Lumière Matière, F-69622 Lyon, France*
[2]*Saint Petersburg Academic University, 8/3 Khlopina Str, St. Petersburg 194021, Russia*
[3]*Lyon Institute of Nanotechnologies INL, CNRS UMR 5270, INSA de Lyon, Université de Lyon, 7 Avenue Jean Capelle, 69621 Villeurbanne cedex, France*
[4]*Centre de Nanosciences et Nanotechnologies, CNRS Université Paris-Saclay, Route de Nozay, F-91460 Marcoussis, France*
[5]*ITMO University, 49 Kronverksky Pr., St. Petersburg 197101 Russia*

(Received 19 June 2017; accepted 10 December 2017; published online 27 December 2017)

We have demonstrated experimentally and theoretically that losses in Tamm plasmon structures can be reduced by using a subwavelength structuration of the metal layer. The structures consist of a GaAs/$Al_{0.95}Ga_{0.05}As$ Bragg reflector covered with a sub-wavelength silver grating. An active quantum dot layer is inserted to perform photoluminescence experiments. Experimental results show that the quality factor of the Tamm plasmon mode with grating increases substantially, with respect to the same structure without a grating. Moreover, a fine-tuning of the Tamm spectral position is obtained by changing the grating parameters. Finite element method simulations are in good agreement with the experimental values. Our results will promote the realization of lasing with the TP based devices at room temperature. *Published by AIP Publishing.* https://doi.org/10.1063/1.4991025

During the past decade, a steady rise of interest has been devoted to Tamm plasmon (TP) based structures due to their potential to achieve lasing, for the fabrication of complex laser arrays and integrated devices. Conventional lasers are based on optical cavities[1] that confine light using mirrors. Tamm plasmon (TP) is a surface electromagnetic state localized at the interface between the metal and the specially designed Bragg mirror.[2] TP modes can be formed in both TM and TE polarizations and present much lower losses than conventional plasmon modes; therefore, TP has found potential applications in the realization of various optical devices based on TP structures.[3–5] The strong coupling regime occurring between a TP mode and an exciton was shown in Refs. 6 and 7. Recently, macroscopic optical coherence,[8] lasing, and polarization-controlled confined Tamm plasmon lasers[9] have been demonstrated.

Despite progress in enhancement of spontaneous emission in TP structures,[10] the main obstacles preventing the improvement of the performance and lasing of TP devices are optical losses[11] and heating of metallic mirrors due to absorption.[12] Even in silver and gold (the noblest metals), absorption is substantial and losses may exceed the achievements on the field confinement. A number of experimental studies on plasmonic devices focus on the reduction of metal losses by structuring the metal layer, which relies on the phenomenon of extraordinary optical transmission[13] through subwavelength metallic structures.[14] The enhanced optical transmission was observed in two-dimensional periodic arrays of holes,[15] and control of TP modes under metallic microdisks was demonstrated.[16,17] An alternative way can be to define a subwavelength grating on the metallic layer. According to effective medium theory (EMT), it offers a possibility to tune the effective refractive index[18–21] of the coating layer and reduce metallic losses.

This paper is aimed at experimental and theoretical investigation of the possibility to reduce losses in the metal layer and to tune the spectral position and quality factor of optical modes in the Tamm plasmon based microcavity by covering the distributed Bragg reflector (DBR) with a periodical silver sub-wavelength grating.

The sample studied in this letter is composed of an active distributed Bragg reflector (DBR) formed by a stack of 30 GaAs/$Al_{0.95}Ga_{0.05}As$ pairs of quarter-wavelength layers grown on a GaAs substrate by molecular beam epitaxy (MBE). The scheme of the structure is illustrated in Fig. 1(a). In the upper high refractive index layer, three InAs monolayers (MLs) were embedded to form quantum dots (QDs) as an active medium. The thickness of the top layer with an active area was designed to locate the TP mode in the center of the photonic bandgap (PBG). The layers of the DBR present a thickness gradient along one of the sample axes, which enables a precise spectral tuning of the modes. In order to realize the subwavelength

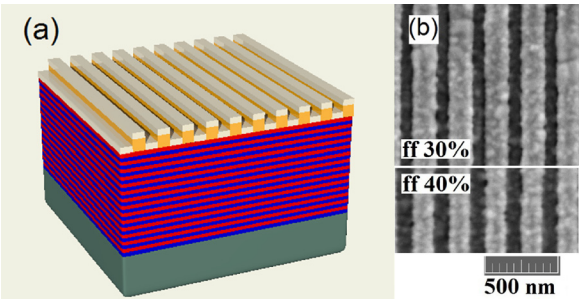

FIG. 1. Schematic structure of the sample (a) and SEM image (b) of the metallic grating.

a)Authors to whom correspondence should be addressed: gubaydullin.azat@gmail.com; joel.bellessa@univ-lyon1.fr; and clementine.symonds@univ-lyon1.fr.

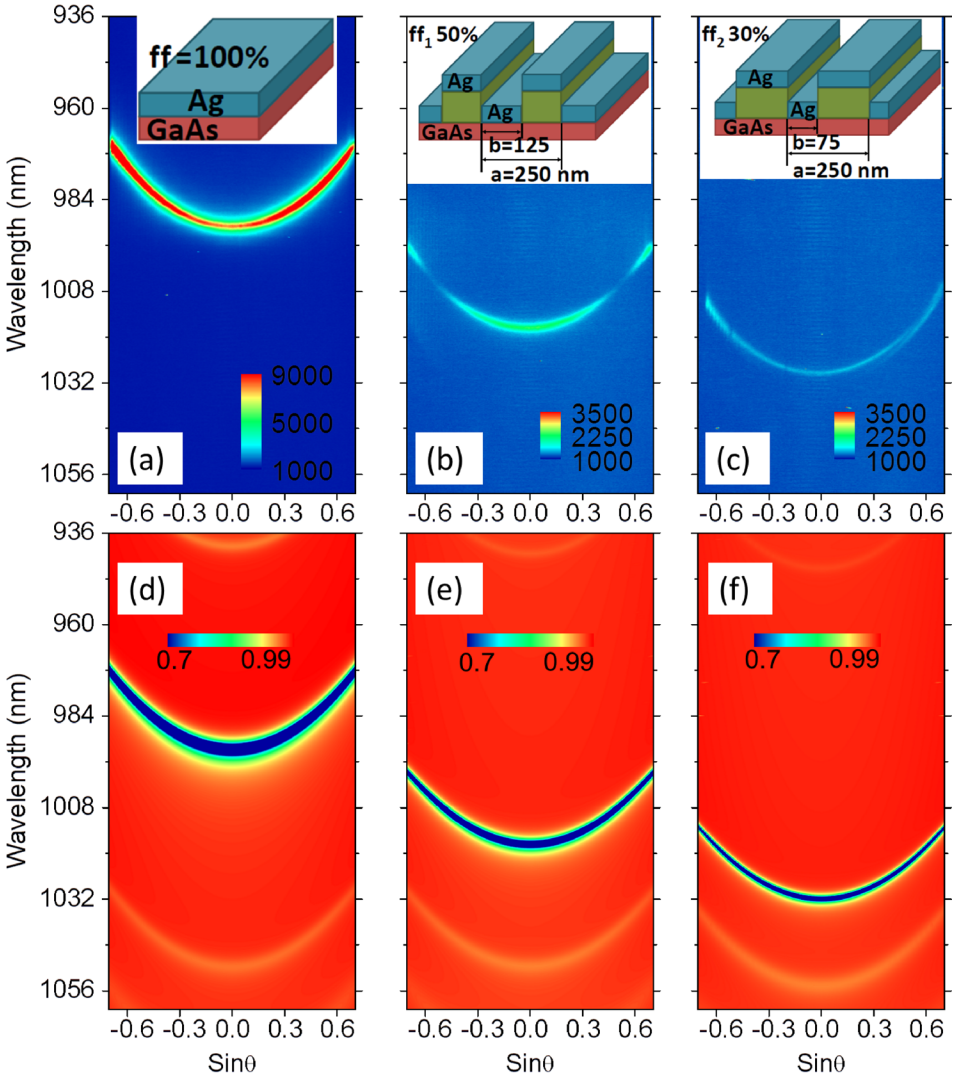

FIG. 2. Experimental emission dispersion relations recorded on the unpatterned device—general Tamm Plasmon (a) and devices covered by silver with a grating characterized by a filling factor of 50% (b) and 30% (c). Reflection calculated by the finite element method (FEM) for devices characterized by a filling factor: (d) 100%, (e) 50%, and (f) 30%.

grating, a 90 nm thick PMMA resist layer was deposited on the top of the DBR and various device patterns with different grating parameters were defined by using e-beam lithography. The grating is defined by two parameters: the period and the filling factor (ff) [see the inset picture in Figs. 2(b) and 2(c)]; SEM images for 30% and 40% ff are presented in Fig. 1(b). On top of the sample, a 45 nm silver layer was thermally evaporated in order to form the Tamm plasmon (TP) mode. No lift-off was performed after the metal deposition, in order to shield from the QD emission coming from outside the targeted area (device) of the sample.

Angular resolved photoluminescence (PL) experiments were performed. The sample was illuminated from the top using a Ti:Sapphire laser operating at 780 nm (pulse duration ~200 fs and repetition rate 80 MHz), focused on the sample surface to a spot with a diameter of ~8 μm, via a long working distance microscope objective. The numerical aperture of the objective lens is 0.75 which corresponds to a $\pm 48^{\circ}$ angular range. The photoluminescence was collected using the same objective and sent to a spectrometer associated with a cooled charged coupled device (CCD). A rotating half-wave plate and a polarizer cube were placed, to be able to measure any linear polarization selectively. The angle resolved reflectivity spectroscopic setup is similar to that described in Ref. 9.

The emission dispersion images recorded at room temperature are presented in Fig. 2. The detected photoluminescence radiation is polarized along the grating grooves. For the unpatterned device (without resist, ff = 100%), the recorded emission pattern is presented in Fig. 2(a) and illustrates a parabolic shape of the Tamm Plasmon mode, characterized by a quality factor of Q = 400. By covering the DBR with a 45 nm silver film with a grating period of 250 nm (below the diffraction limit and is crucial to obtain continuous parabolic dispersion of the TP mode), the quality factor can be increased. The grating allows control over the surface area of the metal/semiconductor interface (direct Ag/GaAs contact), which can be defined by filling factor per period with parameter ***b***, Figs. 2(b) and 2(c). Figure 2(b) shows the emission dispersion recorded on the device with a 50% filling factor, which means that in the period 50% of surface has direct Ag/GaAs contact. The experimentally measured Q factor of the TP mode for this device is Q = 600. While decreasing the surface of metal/semiconductor contact per period of the grating and therefore reducing absorption, the Q factor can be increased up to Q = 970, which is measured on the device with ff = 30%. The corresponding TP mode dispersion is illustrated in Fig. 2(c).

Experimentally measured Q factor values as a function of filling factor are plotted in Fig. 3(a) and indicated with red squares. Error bars are defined from FWHM determination

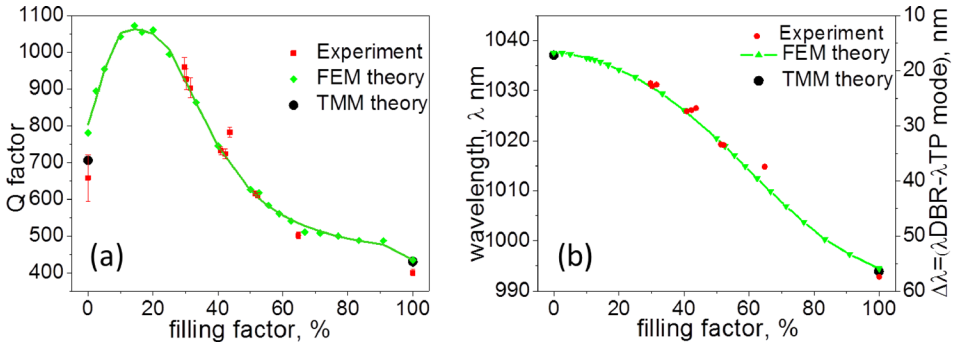

FIG. 3. (a) Experimentally measured quality factor of the Tamm Plasmon mode as a function of filling factor—red squares. The results of 2D FEM simulation are indicated by green symbols. (b) The spectral position of the Tamm Plasmon mode depending on the filling factor: experiment—red circles and FEM theory—green triangles. Black circles indicate values estimated from the reflectivity spectra calculated by the transfer matrix method (TMM).

of the TP emission peaks in the experimental PL spectra at normal incidence by fitting with a Lorenz function. The unpatterned device (ff = 100%) has a Q factor of around 400. The experimental Q factor increases while decreasing the filling factor from 100% to 30%. Interestingly, a decrease to Q = 650 is measured for ff = 0%. This corresponds to the case of an unpatterned sample with a 90 nm resist layer between the DBR and Ag. A first idea is that the decrease in the filling factor leads to a smaller surface of the metal/semiconductor in contact, reducing the metallic losses, which allows the increase in the Q factor.

The position of the TP mode is also modified by the subwavelength structuration over 40 nm, as shown in Fig. 3(b). In this way, a 40 nm wavelength shift is achieved. It allows tuning of the spectral position of the TP mode and future design of the cavity heterostructure similar to those used in the photonic crystal structure.[22] Note that the decrease in the ff leads to an increase in the TP mode wavelength position simultaneously with the variation of its Q factor, in accordance with the dependence shown by the green curve in Fig. 3(a).

The electromagnetic simulations were performed with a finite element method (FEM) using COMSOL Multiphysics. The symmetrical property of the system under consideration allows simulating it with a two-dimensional calculation. The DBR was formed by 30 pairs of GaAs/$Al_{0.95}Ga_{0.05}As$ $\lambda/4$ layers on a GaAs substrate. The thickness of the Ag is 45 nm, and the 90 nm PMMA resist layer was added in accordance with the experimental sample. The thickness of the upper high refractive index layer is chosen to have the TP mode in the center of the PBG.

The refractive indices for each material of the DBR (GaAs/$Al_{0.95}Ga_{0.05}As$) are introduced by functions obtained by fitting experimental data.[23,24] The real part of the frequency-dependent permittivity of the silver is obtained by fitting the Johnson and Christy experimental values.[25] The imaginary part is adjusted to account for the experimentally measured Q factor on the unpatterned TP device [see Fig. 2(a)], since it is shown that the losses in noble metals depend on the method of evaporation[26] and are generally higher at room temperature.[27,28] During simulation, we consider the TE polarization, and we assume that the wave has the electric field component in the y direction, out of the modeling xz-plane.

The angular and spectral dependences of the reflection coefficient calculated by FEM for devices characterized by various filling factors are presented in Fig. 2: (d) 100%, (e) 50%, and (f) 30%. It can be seen that these reflectivity images closely mimic corresponding photoluminescence patterns [Figs. 2(a)–2(c)]. For each device, the edge mode and the Tamm plasmon mode demonstrate parabolic dispersion similar to the one observed in the corresponding emission pattern. Note that the edge mode is more pronounced in the reflection, while in the photoluminescence pattern, the signal is low, since the maximum of the electric field for the edge mode is located in the center of the structure, while for the position of the quantum dot layers, the magnitude of the electric field is similar to the value in uniform media.[10] In both the reflection and the emission patterns, it can be seen that by decreasing the filling factor, the width of the Tamm Plasmon mode is significantly narrowed and its spectral position is strongly varied, while the edge mode is less sensitive to the filling factor variation.

Figure 4 presents the reflectivity spectra (solid) at normal incidence calculated by FEM. The reflectivity spectrum measured experimentally on the device without grating (ff = 100%) is presented by circles; the Tamm Plasmon mode appears as a deeper minimum, and the minimum at higher wavelength is related to the edge state. The Tamm Plasmon modes for each device appear as the deeper minima between 993 and 1037 nm, depending on the filling factor. The dependence of the Q-factor of the TP mode has been estimated from these reflectivity spectra and is shown in Fig. 3(a) by green rhombs, illustrating a very good agreement between theory and experimental results. The solid green curve in Fig. 3(a) is obtained by fitting the Q factor data (green rhombs) estimated from spectra calculated by FEM. The decrease in the filling factor leads to an increase in the Q factor, with a maximum reached around ff = 15%, and for a

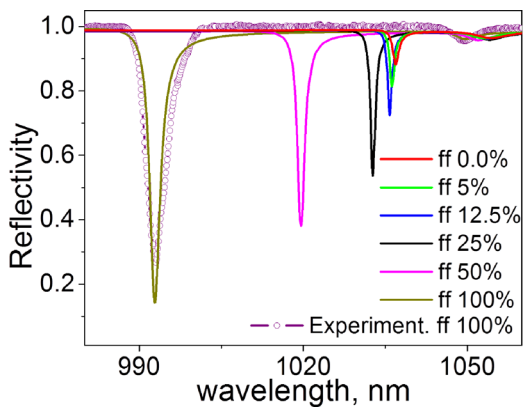

FIG. 4. Reflectivity spectra (solid) of the TP microcavity simulated by FEM for various devices with different metal grating filling factors. The reflectivity spectrum indicated by circles is measured experimentally on the device without grating. All spectra correspond to normal incidence.

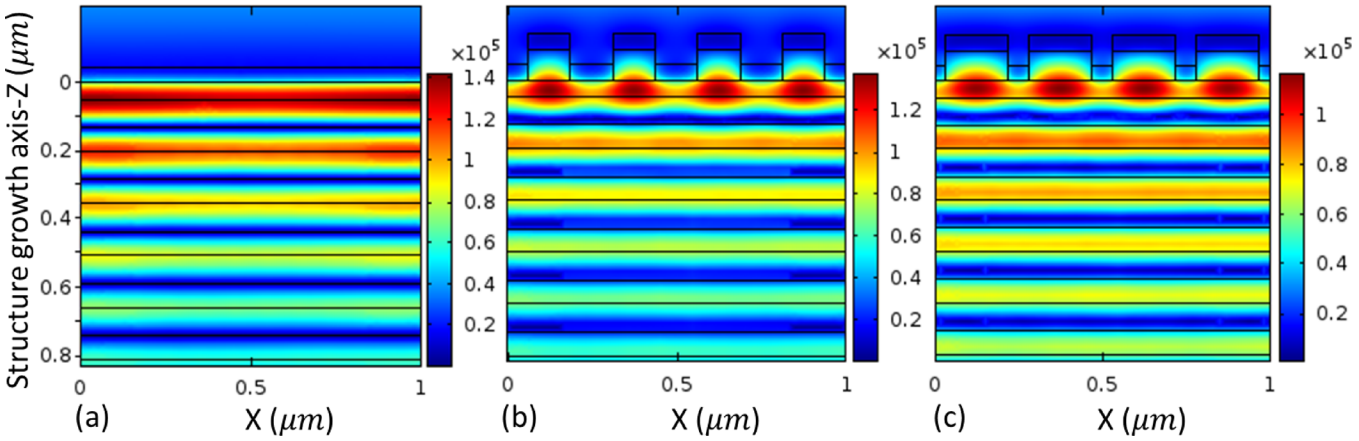

FIG. 5. FEM simulations: norm of the electric field |E| [V/m] of the Tamm Plasmon mode calculated for device 100% covered with Ag—conventional Tamm Plasmon (a), and devices with grating defined by filling factor 50% (b) and 25% (c).

lower ff, a decrease in the Q-factor is observed. This peak illustrates that the Q-factor enhances not just because of the continuous increase in the TP mode wavelength but due to the favorable field confinement, achieved by a sub-wavelength periodical grating, which allows the reduction of losses in the effective coating layer. The spectral position of the TP modes, estimated from FEM calculations, as a function of the ff is presented in Fig. 3(b) by green triangles and also agrees very well with experiments.

Two devices with ff 0% and 100% are planar structures, and therefore, we also performed their simulation with a conventional transfer matrix method (TMM). Reflectivity spectra were calculated by the TMM considering normal light incidence. Estimated values of the Q factor and the TP mode position are indicated in Figures 3(a) and 3(b), respectively, by black circles, illustrating good agreement with FEM results.

To understand the behavior of the losses and the increase in the Q factor of the TP mode with ff variation, the distribution of the electric field norm |E| of the TP mode has been calculated by FEM. Figure 5 shows the spatial distribution along the crystal growth axis-Z, and the horizontal axis-X is parallel to the layer plane. For a device without a grating, presented in Fig. 5(a), the distribution of the electric field in the X direction is uniform. The electric field maximum is located close to the metal/semiconductor interface and decays rapidly in the DBR. For the device with a grating, the field distribution changes, and particularly for ff = 50% [Fig. 5(b)], the lateral evolution of the field in the X direction is now present. It can be observed that the field is predominantly located in the upper Bragg layer, concentrating more under the resist than close to the silver. A similar behavior holds for ff = 25% [Fig. 5(c)], the field is higher under the resist, thus avoiding penetration into the silver. The increase in the quality factor with ff variation observed experimentally can be affected by a localization of the E field under the resist layer, and thus further from metal, which is the lossy part of the system. The quality factor evolution with the filling factor has been reproduced with a Rigorous Coupled Wave Analysis (RCWA) calculation, leading also to a maximum at ff = 20%.

Variation of the Q factor with the filling factor [see Fig. 3(a)] demonstrates a maximum around ff 20%, and such a dependence could be associated with the different loss channels. In our experimental sample with 90 nm resist, in the device with ff = 0%, losses are associated with the bottom of the DBR; the electric field in this case has a Gaussian envelope. Then, for ff = 20%, losses from the metal and the bottom DBR are equal, resulting in the maximum Q-factor around ff = 20%. Then, increasing ff > 20%, the losses associated with the metal become dominant. We also note that the variation of the thickness of the resist layer until a particular value can lead to an enhancement of the Q factor. The sub-wavelength structuration method allows the combination of two Tamm plasmon resonances (with resist layer and without it) in a single structure, therefore allowing smooth and precise tuning of the TP mode spectral position without a great decrease in the quality factor of the TP mode. Such precise tuning of the TP mode spectral position allows designing a structure to achieve a targeted field confinement, which is crucial for the formation of the cavities.[22]

We have demonstrated experimentally and theoretically the enhancement of the quality factor of the Tamm plasmon mode by structuration of the metal coating layer, applying periodical (subwavelength) grating. By measuring the angle resolved photoluminescence at room temperature of the Tamm plasmon structures formed by GaAs/$Al_{0.95}Ga_{0.05}As$ DBR with embedded InAs QDs in the active area, we have shown that the quality factor of the TP mode measured on the device with the grating increases substantially, with respect to the same TP microcavity without the grating. We have performed simulations of the reflectivity spectra of the TP microcavity using the 2D finite element method and shown that the variation of the metal grating parameters allows spatial control of the Tamm plasmon mode and enhancement of its Q factor, illustrating good agreement with experimentally observed results. The possibility to control the spectral position of the TP mode makes it able to achieve smooth confinement.

This work was supported by HyMeCav Project. C.S. and J.B. acknowledge financial support from Agence Nationale de la Recherche (ANR) on ANR Project NEHMESIS. A.G. and M.K. acknowledge financial support by Russian Science Foundation Grant No. 16-12-10503.

[1]K. J. Vahala, Nature **424**, 839 (2003).
[2]M. Kaliteevski, I. Iorsh, S. Brand, R. A. Abram, J. M. Chamberlain, A. V. Kavokin, and I. A. Shelykh, Phys. Rev. B **76**, 165415 (2007).
[3]T. Goto, A. V. Dorofeenko, A. M. Merzlikin, A. V. Baryshev, A. P. Vinogradov, M. Inoue, A. A. Lisyansky, and A. B. Granovsky, Phys. Rev. Lett. **101**, 113902 (2008).
[4]M. E. Sasin, R. P. Seisyan, M. A. Kalitteevski, S. Brand, R. A. Abram, J. M. Chamberlain, A. Y. Egorov, A. P. Vasil'ev, V. S. Mikhrin, and A. V. Kavokin, Appl. Phys. Lett. **92**(25), 251112 (2008).
[5]M. Salewski, S. V. Poltavtsev, Y. V. Kapitonov, J. Vondran, D. R. Yakovlev, C. Schneider, M. Kamp, S. Höfling, R. Oulton, I. A. Akimov, A. V. Kavokin, and M. Bayer, Phys. Rev. B **95**, 035312 (2017).
[6]C. Symonds, A. Lemaître, E. Homeyer, J. C. Plenet, and J. Bellessa, Appl. Phys. Lett. **95**, 151114 (2009).
[7]N. Lundt, S. Klembt, E. Cherotchenko, S. Betzold, O. Iff, A. V. Nalitov, M. Klaas, C. P. Dietrich, A. V. Kavokin, S. Höfling, and C. Schneider, Nat. Commun. **7**, 13328 (2016).
[8]R. Brückner, A. A. Zakhidov, R. Scholz, M. Sudzius, S. I. Hintschich, H. Frob, V. G. Lyssenko, and K. Leo, Nat. Photonics **6**(5), 322 (2012).
[9]G. Lheureux, S. Azzini, C. Symonds, P. Senellart, A. Lemaître, C. Sauvan, J.-P. Hugonin, J.-J. Greffet, and J. Bellessa, ACS Photonics **2**, 842 (2015).
[10]A. R. Gubaydullin, C. Symonds, J. Bellessa, K. A. Ivanov, E. D. Kolykhalova, M. E. Sasin, A. Lemaître, P. Senellart, G. Pozina, and M. A. Kaliteevski, Sci. Rep. **7**, 9014 (2017).
[11]J. B. Khurgin, Nat. Nanotechnol. **10**(1), 2–6 (2015).
[12]A. D. Rakić, A. B. Djurišic, J. M. Elazar, and M. L. Majewski, Appl. Opt. **37**, 5271–5283 (1998).
[13]T. W. Ebbesen, H. J. Lezec, H. F. Ghaemi, T. Thio, and P. A. Wolff, Nature **391**(6668), 667 (1998).
[14]F. Medina, J. A. Ruiz-Cruz, F. Mesa, J. M. Rebollar, J. R. Montejo-Garai, and R. Marques, Appl. Phys. Lett. **95**, 071102 (2009).
[15]F. J. García-de-Abajo, Rev. Mod. Phys. **79**, 1267 (2007).
[16]O. Gazzano, S. M. de Vasconcellos, K. Gauthron, C. Symonds, J. Bloch, P. Voisin, J. Bellessa, A. Lemaître, and P. Senellart, Phys. Rev. Lett. **107**, 247402 (2011).
[17]C. Symonds, G. Lheureux, J. P. Hugonin, J. J. Greffet, J. Laverdant, G. Brucoli, A. Lemaître, P. Senellart, and J. Bellessa, Nano Lett. **13**(7), 3179–3184 (2013).
[18]H. Kikuta, Y. Ohira, H. Kubo, and K. Iwata, J. Opt. Soc. Am. A **15**, 1577–1585 (1998).
[19]X. Xu, H. Subbaraman, J. Covey, D. Kwong, A. Hosseini, and R. T. Chen, Appl. Phys. Lett. **101**, 031109 (2012).
[20]S. Brand, R. A. Abram, and M. A. Kaliteevski, Phys. Rev. B **75**, 035102 (2007).
[21]Z. Wang, X. Xu, D. Fan, Y. Wang, H. Subbaraman, and R. T. Chen, Sci. Rep. **6**, 24106 (2016).
[22]C. Jarlova, A. Lyasota, L. Ferrier, P. Gallo, B. Dwir, A. Rudra, and E. Kapon, Appl. Phys. Lett. **107**, 191101 (2015).
[23]A. D. Rakić and M. L. Majewski, J. Appl. Phys. **80**, 5909–5914 (1996).
[24]T. Skauli, P. S. Kuo, K. L. Vodopyanov, T. J. Pinguet, O. Levi, L. A. Eyres, J. S. Harris, M. M. Fejer, B. Gerard, L. Becouarn, and E. Lallier, J. Appl. Phys. **94**, 6447–6455 (2003).
[25]P. B. Johnson and R. W. Christy, Phys. Rev. B **6**, 4370 (1972).
[26]D. E. Aspnes, E. Kinsbron, and D. D. Bacon, Phys. Rev. B **21**, 3290 (1980).
[27]J. A. McKay and J. A. Rayne, Phys. Rev. B **13**, 673 (1976).
[28]J.-S. G. Bouillard, W. Dickson, D. O'Connor, G. Wurtz, and A. Zayats, Nano Lett. **12**, 1561 (2012).